Atomization and Sprays, vol. 5, pp. 417–433, 1995

ATOMIZATION OF CROSS-INJECTING SPRAYS INTO CONVECTIVE AIR STREAM

K. D. Kihm, G. M. Lyn, and S. Y. Son
Department of Mechanical Engineering, Texas A&M University, College Station, Texas

Experimental investigations have been made for cross-injecting sprays into a convective air stream as a primary means of fuel atomization. A laser diffraction particle-analyzing technique (the Malvern system) is used assuming a Rosin-Rammler two-parameter model for the drop size distribution function. The study's varied injection parameters include the convective air flow rate, the flow rate of the injected liquid (distilled water), the orifice diameter, and measurement locations along the two-dimensional spray plane. Buckingham-PI analysis finds the correlation of dimensionless parameters. A correlation of drop Sauter mean diameter (SMD) normalized to the orifice diameter is obtained from all the experimental data as

$$\frac{\mathrm{SMD}}{D_o} = 1.015 \times 10^{19}\, \mathrm{Re}_g^{-3.5998}\, \mathrm{Re}_f^{-1.8094}\, \mathrm{We}^{2.2474} \left(\frac{x}{D_o}\right)^{-0.6867} \left(\frac{y}{D_o}\right)^{1.9718}$$

where D_o is the injector orifice diameter that constitutes the length scale of Re_f and of We. The air Reynolds number, Re_g, is defined based on the channel hydraulic diameter. A statistical analysis of the correlation equation shows a 97.5% confidence interval and a coefficient of multiple determination, R^2, of 0.94.

INTRODUCTION

A liquid fuel jet in a crossing gas flow can be a practical alternative for fuel injection in combustion processes (Fig. 1). This is more so because of one important physical characteristic of the jet in a cross flow. As the liquid jet penetrates the gas flow and atomization takes place, larger drops tend to move out farther into the air stream than smaller drops, because of the greater momentum of the larger drops [1]. The resulting spray drop size distribution will increase monotonically farther away from the injector orifice. This unique feature of cross-injecting sprays makes it possible to control the drop size spectrum actively, by limiting the maximum and minimum drop sizes.

Cross-injecting sprays also have a particular advantage for slurry-type fuel injection, where severe injector wear and frequent nozzle clogging are anticipated. Severe wear and frequent clogging of conventional pressure atomizers are major problems when considering CWS fuel usage for combustion applications such as gas turbines and diesel engines [2]. The injector wear and clogging occur primarily because of the high-pressure injection of the pressure atomizer required to provide an appropriate atomization efficiency, i.e., sufficiently fine drops. For the case of cross injection, however, a fuel jet at a low injection pressure induces atomization because of the tearing action of the high-speed convective gas flow, which reduces the possibility of clogging and wearing of the nozzle.

The present work was supported by the U.S. Department of Energy, Pittsburgh Energy Technology Center, Contract No. DE-FG22-92PC92156. The authors would like to acknowledge gratefully Dr. Soung S. Kim, Technical Project Monitor at DOE-PETC.

NOMENCLATURE

ALR	air-to-liquid ratio	x	coordinate parallel to the air flow, mm
D_H	channel hydraulic diameter, mm	y	coordinate perpendicular to the air flow, mm
D_o	orifice diameter, mm	μ	dynamic viscosity, kg/m s
D_{30}	number mean diameter of drops, μm	ν	kinematic viscosity, m^2/s
l	orifice length, mm	ρ	density, kg/m^3
Re_f	Reynolds number for injected water ($= \rho_f V_f D_o/\mu_f$)	σ	surface tension coefficient, N/m
Re_g	Reynolds number for air flow ($= \rho_g V_g D_H/\mu_g$)		**Subscripts**
SMD	Sauter mean diameter, μm	f	liquid (distilled water)
V	gas or liquid velocity, m/s	g	gas (air)
We	Weber number ($= \rho_g V_g^2 D_o/\sigma$)		

It appears that liquid jet breakup may occur in several modes [3]. These modes depend on such factors as nozzle or injector geometry, relative velocity of the jet to the gas into which it is injected, and physical properties of the gas and the injected liquid. A liquid jet disintegration has three parts [4]: (1) Rayleigh breakup without ligament formation, where mean drop diameter is roughly the jet diameter and maximum drop diameter is about twice the jet diameter; (2) formation of membrane ligaments from round jets based on Kelvin-Helmholtz wave development (drop diameters are considerably smaller than the jet diameter); and (3) fibrous ligaments form on the liquid surfaces and are peeled off and break into drops. Drop diameters are an order of magnitude smaller than the jet diameter.

Relating Chigier's model to a jet in a cross flow requires the schematic illustration in Fig. 2. The jet cross section changes from circular to kidney-shaped as the jet exits the orifice into the airflow. Two counterrotating vortices parallel to the jet appear on its lee side and gradually dominate the dynamics of the surrounding fluid. The jet also begins to bend in the direction of the wind. In the second phase, waves caused by the column instability of the jet start to form on the liquid surface and, when amplified by the air flow, shed into ligaments. This is the initiation of the third phase that rapidly collapses to form drops [5].

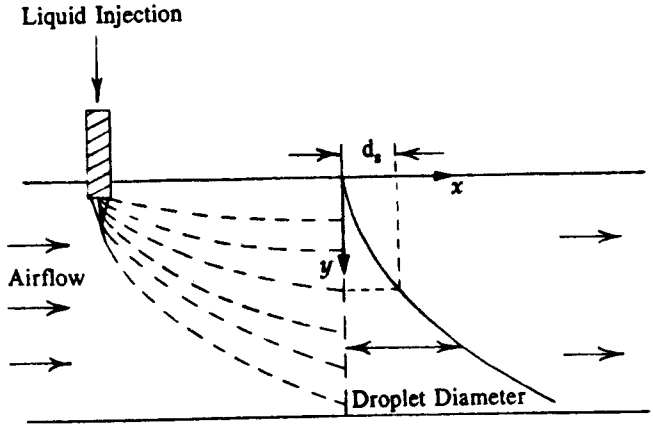

Fig. 1 Schematic drop size distribution of a cross-injecting spray.

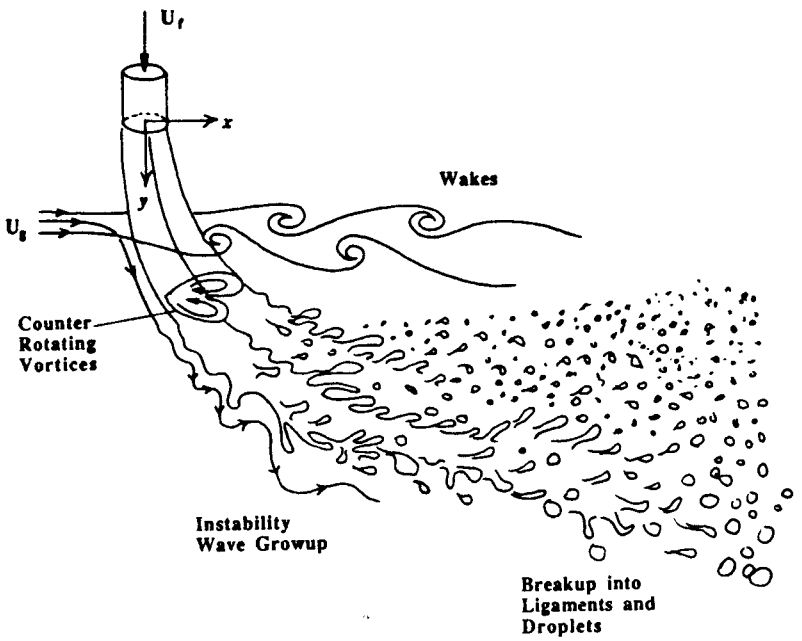

Fig. 2 Atomization model for cross-injecting liquid jet into a convective air flow.

Many experiments and mathematical modelings have investigated the structure, trajectory, and mixing rate of transverse jets. The literature survey can go as early as 1957, when Ingebo and Foster [1] showed the physical characteristics of cross-injecting sprays experimentally. Keffer and Baines [6] experimented with various jet strengths and the position of the jet when stretched by the ratio of jet-to-crosswind momenta to come up with a single descriptive function. Adelberg [3, 5] investigated mean drop size, breakup rate, and penetration of cross-injecting sprays extensively. Kamotani and Greber [7] reported on experiments of circular jets issuing into a cross flow. Moussa et al. [8] studied the near field in the mixing of a round jet with a cross stream. Broadwell and Breidenthal [9] analyzed the structural and mixing characteristics of cross injection. Andreopoulos [10] used spectral analysis and flow visualization to study the structure. Heister et al. [11] incorporated analytical and numerical modeling in the study of a jet in subsonic and supersonic cross flows. Needham et al. [12, 13] derived equations representing a jet in a cross flow. Askari et al. [14] used a remote-sensing laser system and a finite-difference model to look at the concentration of a turbulent jet. Li and Karagozian [15] predicted the breakup of a liquid jet in supersonic cross flow. Benson and Kim [16] calculated a three-dimensional turbulent flow of a jet in a cross flow using a multiple-time-scale turbulence model and experimented with opposed jets discharging normally in a cross stream. Higuera and Martinez [17] described the incipient bending of a round incompressible jet.

Although there are many excellent articles in the literature, it is surprising that only a handful of studies are available for the drop size characteristics for such widely studied cross-injecting sprays. Ingebo and Foster [1] were first to study a liquid jet in a cross air flow systematically. A combined high-speed camera and sampling technique obtained data over ranges of injectors, injected liquids, and air flow variables. Although the study showed

visually that drop sizes were spatially dependent, quantitative results were available only for a spatially averaged drop size correlation:

$$\frac{D_{30}}{D_o} = 3.9(\mathrm{We}\,\mathrm{Re})^{-0.25} \tag{1}$$

In the preceding equation $\mathrm{We} = \rho_g D_o V_g^2/\sigma$ and $\mathrm{Re} = D_o V_g/\nu_f$, where σ and ν_f are the surface tension and kinematic viscosity, respectively, of the liquid, and V_g and ρ_g are the free-stream velocity and density, respectively, of the air. The length scale was selected as the orifice diameter D_o.

A series of analytical work by Adelberg [3, 5] predicted the mean drop size generated by a liquid jet penetrating a high-speed gas stream. The primary drop generation was dominated by either capillary action or acceleration forces. These were typical of those reported in the literature where the free-stream dynamic pressure exceeds 14.5 kPa in gauge (2.1 psig), and acceleration rather than capillary waves dominate the breakup mechanism. The analysis for the mean drop size for acceleration wave breakup results in the following equation:

$$D_{30} = 65.3\left[\frac{\mu_f\left(\sigma/\rho_f\right)^{1/2}}{\rho_g V_g^2}\right]^{2/3} \tag{2}$$

In exploring cross-injecting sprays as a more effective atomization method with active control over the drop sizes, it is necessary to find a more comprehensive correlation with the spatial variations of drop diameters. The goal of the present study is to establish an experimental correlation of spatial drop size distribution in terms of other operation parameters of cross injection, including gas Reynolds numbers, liquid injection rate, Weber numbers, x coordinate, y coordinate, and injector orifice diameter.

EXPERIMENTAL APPARATUS

Test Channel

Figure 3 illustrates schematically the cross-injecting atomizer system. The test channel is fabricated from Plexiglas. Two glass viewing windows conform to the side walls and allow spray visualization and optical access of the drop sizing system. The channel has a 25 × 33 mm cross section and is approximately 914 mm long, which ensures fully developed flow near the end of the channel where the injection nozzle is found. The entire channel is laid on a two-dimensional positioning system, which allows precise spatial location of measurement. A bypass control plate placed on the blower outlet adjusts the air flow rate. An orifice flow meter installed 5 ft upstream of the channel inlet measures the air flow rate. A Kiel probe (a type of Pitot tube) measures the mean velocity profiles across the y coordinate and shows excellent agreement with the one-seventh-law velocity profile for fully developed turbulent flows. The 1.5-hp fan blower provides air Reynolds numbers ranging from 20,000 to 75,000 based on the 28.4-mm length scale of the channel hydraulic diameter. Distilled water is the atomized liquid, and the flow rate is measured with a calibrated rotameter.

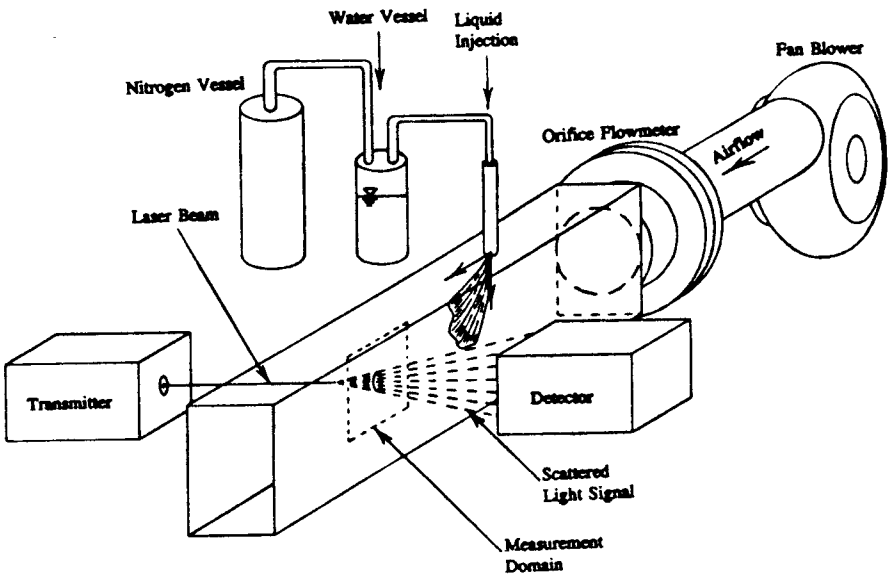

Fig. 3 Schematic illustration of experimental system.

Injector Nozzle

Regulated nitrogen gas pressurizes the liquid reservoir and drives the liquid at constand injection pressure. Five different injectors (0.2-, 0.3-, 0.4-, 0.5-, and 0.6-mm orifice diameter) are tested in the experiment. The injectors are made of aluminum rod material (Fig. 4) with external dimensions of 9.5 mm outside diameter by 64.8 mm long. The orifice length-to-hole diameter ratio, l/D_o, is 10.0 for all the injectors, so the inside geometric effect on the atomization between injectors can be small [18]. The orifice exit was protruded from the duct wall by approximately 2 mm. The air velocity calculated with the one-seventh law at the orifice exit location (y = 2 mm) approached nearly 80% of the maximum centerline velocity, and the effect of the decelerated flow near the duct wall was considered small.

Diagnostic Equipment

A high-speed photographic recording provides instantaneous visualization of the sprays to examine the characteristics of the jet entering the cross flow and the subsequent atomization downstream of the initial breakup. One-half-microsecond pulsed lighting of the Microflash system illuminates the spray, and a standard 35-mm camera with a macro extension lens magnifies the view. The photographic recording of the sprays has successfully guided the drop diameter measurement taken downstream of the breakup region to eradicate erroneous data that occur due to the presence of ligaments or nonspherical drops.

The Malvern 2600C laser diffraction particle sizer measures the drop sizes. To enhance the spatial resolution of the measurement, the standard laser beam diameter of 9 mm has been reduced to 4.5 mm by replacing the transmitting lens with one with a shorter focal length [19]. Case has been taken to minimize the data biasing due to the multiple

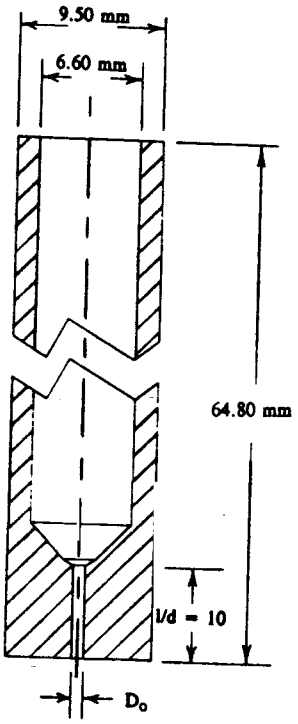

Fig. 4 Cross-sectional view of injector orifice.

reflections of the beam passing the two side windows. This has been achieved by aligning the test channel windows slightly off the right angle with the laser beam. The modified Malvern instrument has been satisfactorily calibrated using a standard calibration reticle.

RESULTS AND DISCUSSION

Table 1 shows the test conditions investigated with distilled water as an injected liquid. The measurement conditions include five different orifice diameters ranging from 0.2 to 0.6 mm, three different Reynolds number of 50,000, 60,000, and 70,000, and two different x locations of 10 and 20 mm from the nozzle orifice center. The range in the y direction extends to the spray boundary that gives 1% or higher light obscuration and allows the Malvern measurement. Measurement farther downstream than $x = 20$ mm is not possible because of window wetting of the deposition of spray drops. The high momentum of the injected liquid beyond a certain limit makes the stream penetrate to the opposite wall without developing a noticeable spray. At the other extreme, if air momentum is too strong compared with that of the liquid jet, the spray is quenched down to the upper channel surface and no measurement is possible. The Malvern detector receives the scattered light energy at a rate of 600 sweeps for each measurement condition. The detected energy distribution is fitted using a Rosin-Rammler two-parameter model to find necessary statistical information on drop sizes.

Table 1 Test Matrix of Experimental Conditions

	Orifice diameter (mm)	Air-to-liquid ratio (ALR)	Liquid flow rate (ml/s)	x (mm)
Base case	0.4	Re = 70,000	0.79–2.63	10
Liquid flow rate (ml/s)	0.5	25	2.10, 2.52, 2.94	10
	0.6	25	2.10, 2.52, 2.94	10
Orifice diameter (mm)	0.2	Re = 70,000	0.79	10
	0.3	Re = 70,000	0.79–1.58	10
	0.5	RE = 70,000	1.58–4.21	10
	0.6	Re = 70,000	1.58–5.26	10
ALR	0.5	25, 30, 35	2.10	10
	0.6	25, 30, 35	2.10	10
x (mm)	0.3	Re = 70,000	0.79	20
	0.4	Re = 70,000	0.79–1.58	20

The error analysis has been carried out using the Kline-McKlintok error analysis method [20]. Detailed analysis is presented elsewhere [21], and the estimate shows drop Sauter mean diameter (SMD) uncertainties of approximately ±6.7%. In addition, the Malvern calibration with the calibration reticles gives equipment accuracy at nearly ±4.0%. The root mean square of these two uncertainties is ±7.8%, so the maximum uncertainties of the experiment do not exceed a very conservative estimate of 10%.

Figure 5 shows spray drop size distributions measured for three different y coordinates at x = 10 mm downstream of the 0.6-mm-diameter nozzle injecting distilled water at a rate of 3.68 ml/s, and Re_g = 60,000. As the y location increases, the peak of the size

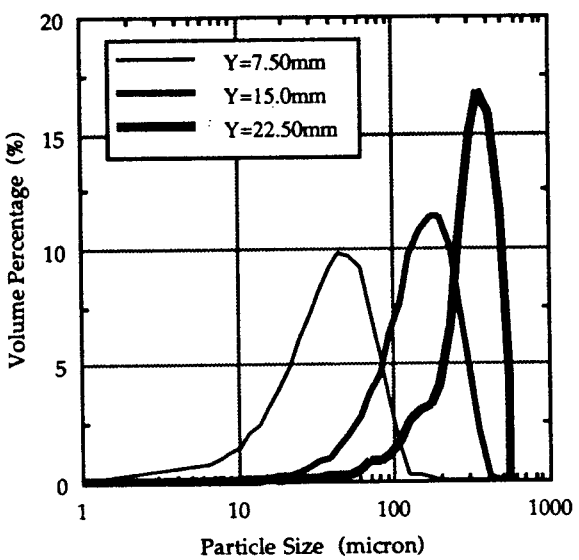

Fig. 5 Drop size distribution functions measured at different y locations: x = 10 mm, D_o = 0.6 mm, $\dot{m}_f$ = 3.68 ml/s, and Re_g = 60,000.

distribution clearly shifts toward a larger median diameter. Such transition of the peak of the size curve is observed consistently for all results obtained for other experimental conditions. This indicates that larger drops with high inertia-to-drag ratios penetrate deeper in the y direction than smaller drops.

Correlation of SMD

A functional relation between the injection parameters is established based on Buckingham-PI analysis. Detailed analyses are presented in the Appendix. By employing a regression method for all the SMD data, an experimental correlation of the Buckingham-PI dimensionless parameters is

$$\frac{\text{SMD}}{D_o} = 1.015 \times 10^{19}\, \text{Re}_g^{-3.5998}\, \text{Re}_f^{-1.8094}\, \text{We}^{2.2474} \left(\frac{x}{D_o}\right)^{-0.6867} \left(\frac{y}{D_o}\right)^{1.9718} \tag{3}$$

where D_o is the injector orifice diameter that constitutes the length scale of Re_f and of We. The air Reynolds number, Re_g, is defined based on the channel hydraulic diameter D_H. In examining the exponent of the Weber number, which is defined as $\rho_g V_g^2 D_o/\sigma$, SMD decreases with increasing surface tension. This contradicts what is generally observed n conventional air-blast atomization, where SMD increases with increasing surface tension. The way to change the Weber number in the current study, however, is to alter either the gas velocity or the orifice diameter. Increasing gas velocity or orifice diameter, which increases the Weber number, will reduce the spray penetration and decrease the shearing area and make atomization less effective, resulting in larger drop SMDs. This unique characteristic of the jet in a cross flow is discussed in more detail by looking at the individual effect, one at a time, with other conditions fixed in the subsequent sections.

Figure 6 compares the experimental results with the calculated values from the correlation. A statistical analysis of the correlation equation shows a 97.5% confidence interval and a coefficient of multiple determination, R^2, of 0.94. The R^2 value is an indicator of the correlation accuracy ranging from 0 to 1.0, where 1.0 denotes a perfect correlation.

Effect of Liquid Injection Rate

The 0.4-mm injector orifice is first tested to establish a "base" case of the gas Reynolds number of 70,000, x = 10.0 mm, and a water flow rate varying from 0.79 to 2.63 ml/s. The y coordinate is varied in 2.5-mm increments from 7.5 to 25 mm. The measurements stop when the obscuration level falls below 1.0% or wetting on the glass panels starts biasing the data. Also, the log difference values of good data should not exceed the acceptable value of 5.0. All results are presented in terms of normalized Sauter mean diameter (SMD/D_o) versus normalized y coordinate, y/D_o.

Figure 7 shows the results for the base case. The experimental data shown with symbols agree fairly well with the correlation curves. Spray SMDs consistently exhibit a monotonic increase with increasing y because of the higher penetration of larger drops. Spray development is also captured photographically using 0.5-μs pulsed lighting generated from a microflash. Typical examples are presented in the three inserted photographs. The three pictures have identical spray conditions except for the liquid flow rate. For the lower liquid rate of 0.79 ml/s, the potential core of the jet does not penetrate the air flow

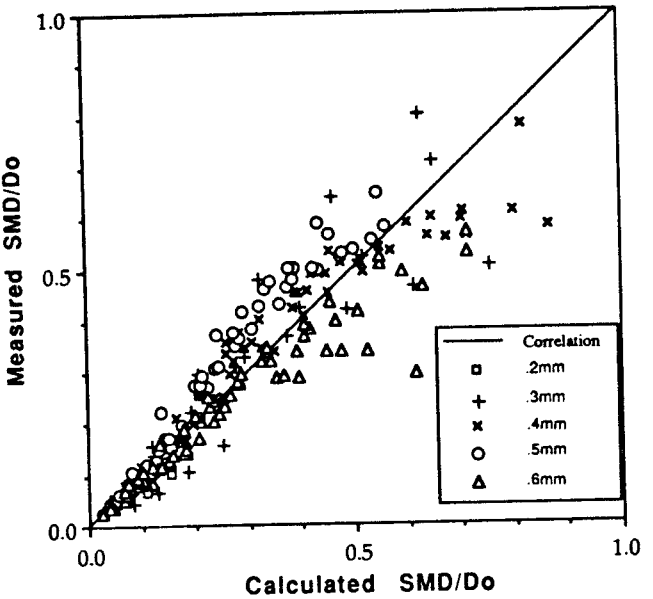

Fig. 6 Comparison of measured SMDs with correlation for different orifice diameters.

as deeply as the others. Breakup occurs almost immediately after the water is injected. The jet's surface tension forces are quickly overcome by the shearing forces of the air stream that eventually generates drops. As the water flow rate increases, the jet's inertia increase allows a deeper penetration and longer potential core into the air stream.

Note that the spray drop SMDs increase with a decreasing liquid flow rate for a specified air flow rate or equivalently increasing air-to-liquid ratio (ALR). It is known that increasing ALR reduces spray mean diameters for the case of conventional axial atomizers. Drop size distribution of the present cross-injecting atomizer, however, shows more sophisticated spatial resolution. The SMD distribution is closely correlated with the physical development of the spray and its penetration. The spray penetration increases consistently with an increasing liquid flow rate. The spray cross section, where air blasting and shear energy exchange actively occur between air and liquid, has increased with increasing spray penetration or equivalently with increasing liquid flow rate. As a result, more effective atomization, i.e., finer SMDs, are observed with increasing liquid flow rate, which in turn decreases ALR. The increased momentum or shear energy of the increased liquid flow rate contributes additionally to reduce the drop SMDs.

Figures 8 and 9 show similar effects of liquid injection rate on drop SMDs for 0.5- and 0.6-mm orifice diameters, respectively, and other conditions the same as in Fig. 7, that is, $x = 10$ mm and $Re_g = 70{,}000$. For both cases, an increasing injection rate decreases SMD because of the deeper spray penetration into the crossing air stream, as discussed previously. The correlations show better agreement with measured SMDs when the liquid injection rate is higher and well-developed sprays are expected. The discrepancies shown for lower injection rates are attributed to the incomplete development of the injected spray due to the excessive air-stream inertia over the injection momentum.

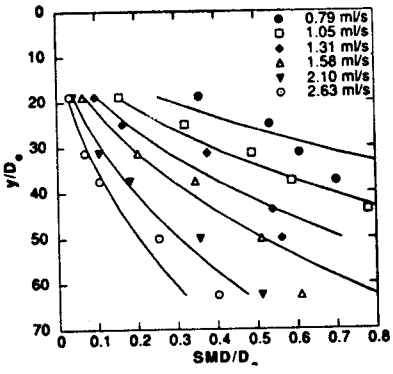

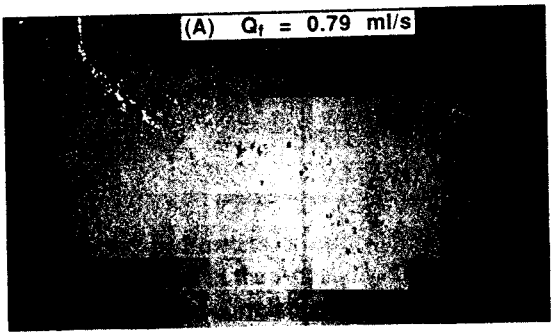

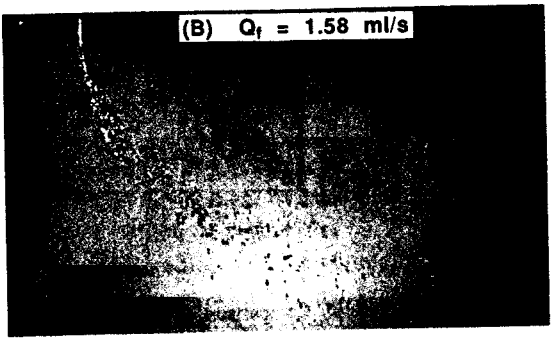

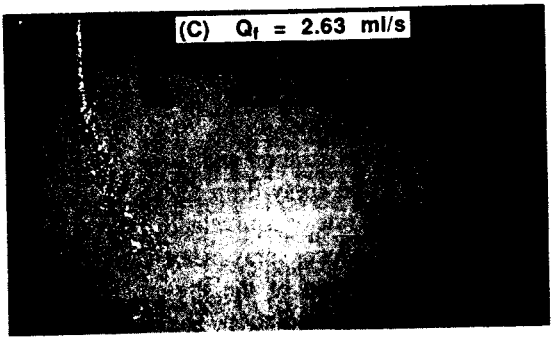

Fig. 7 SMD versus y for different $\dot{m}_f$ ranging from 0.79 to 2.63 ml/s: x = 10 mm, D_o = 0.4 mm, and Re_g = 70,000.

Effects of Orifice Diameter

Figure 10 shows a comparison of the 0.2-, 0.3-, and 0.4-mm nozzle cases at a fixed water flow rate of 0.79 ml/s. The corresponding Reynolds numbers based on the orifice diameter, $Re_f = \rho_f V_f D_o/\mu_f$, are 5,030, 3,353, and 2,515, respectively. The larger orifice diameter under a fixed flow rate reduces the injection velocity, which in turn decreases the liquid jet momentum and its penetration. The spray photographs show clearly the dependence of the spray penetration on the nozzle size. The reduction of the spray cross section facing the air flow with increasing orifice diameter can explain the dramatic increase of SMD with D_o shown in Fig. 10.

When the injection velocities are adjusted to be approximately identical for two different orifices under the same gas Reynolds number, i.e., under the condition of nearly

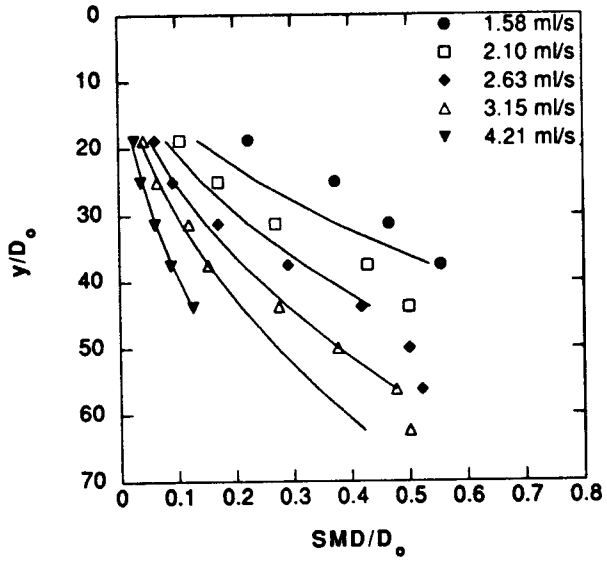

Fig. 8 SMD versus y for different $\dot{m}_f$ ranging from 1.58 to 4.21 ml/s: x = 10mm, D_o = 0.5 mm, and Re_g = 70,000.

identical relative velocity (25 ± 1 m/s) of the gas to liquid in Fig. 11, the dramatic discrepancies in Fig. 10 have been reduced significantly. It seems that the amount of the relative gas-to-liquid velocity is a dominant parameter in finding the atomization of cross-injecting sprays.

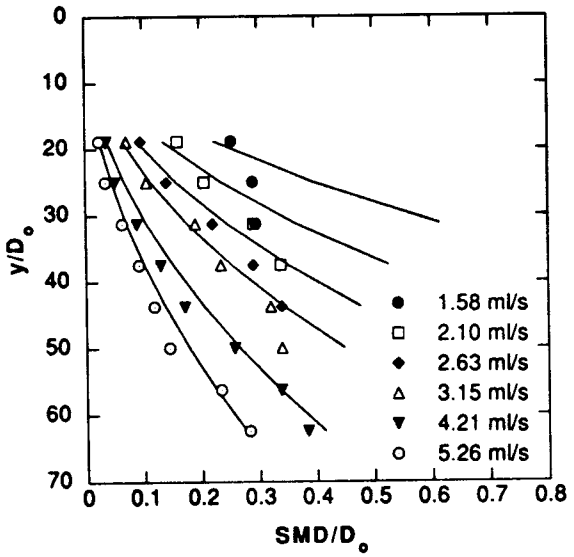

Fig. 9 SMD versus y for different $\dot{m}_f$ ranging from 1.58 to 5.26 ml/s: x = 10 mm, D_o = 0.6 mm, and Re_g = 70,000.

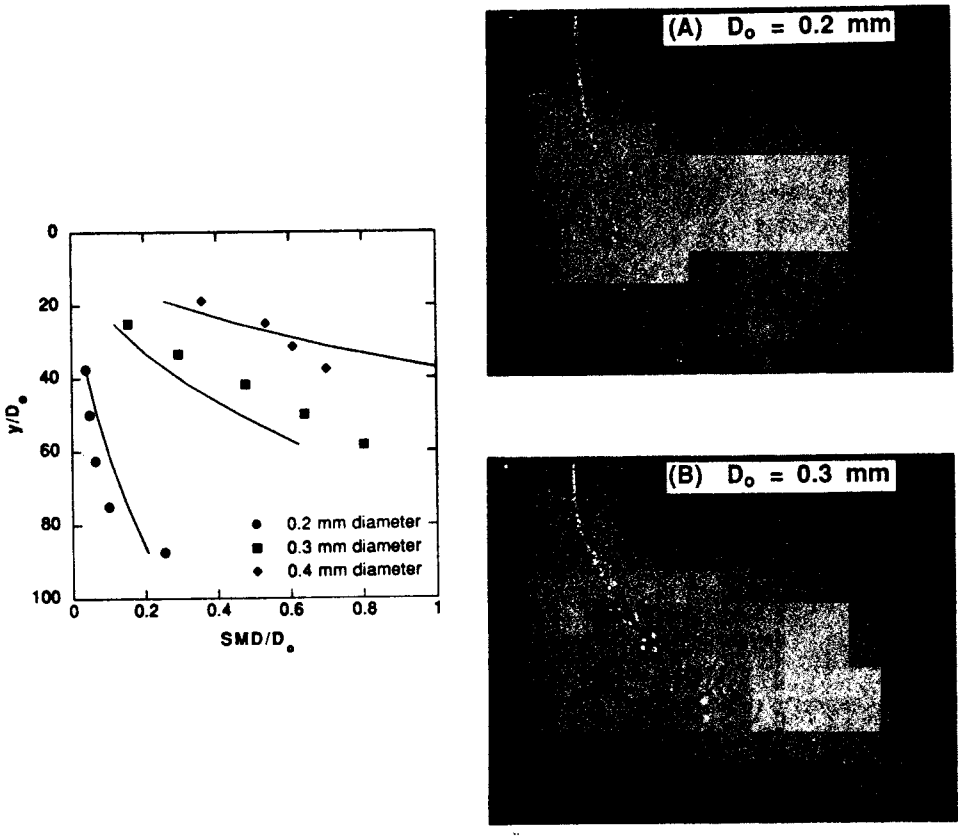

Fig. 10 SMD versus y for different orifice diameters measured at x = 10 mm, $\dot{m}_f$ = 0.79 ml/s, and Re_g = 70,000.

Effects of Air-to-Liquid Ratio

Two separate conditions are tested. The first keeps the air-to-liquid ratio (ALR) constant at 25.0 while varying the air-flow Reynolds number to 50,000, 60,000, and 70,000 with water flow rate accordingly at 2.10, 2.52, and 2.94 ml/s injected through the 0.5-mm-diameter orifice (Fig. 12). The same ALR results in a single value of the momentum ratio of air flow to liquid flow, and the photographic observations for the three cases show similar spray development and penetration. The momentum ratio of the two fluids apparently determines the spray penetration. However, the spray SMD shows a gradual decrease with an increasing amount of both fluids. For a larger liquid flow rate under the same ALR, the air velocity increases in greater degree than the liquid velocity because of the large density difference between air and water. This results in increased momentum transfer per unit liquid mass and leads to a reduced SMD as the liquid injection rate is increased while keeping the ALR unchanged. Again, the relative air velocity with respect to water plays an important role in finding SMD. This is consistent with the previous finding in two-dimensioonal air-blast atomization [22].

In the second variation, ALR is varied from 25 to 35 while keeping other parameters fixed (Fig. 13). The corresponding air-flow Reynolds numbers are 50,000, 60,000, and

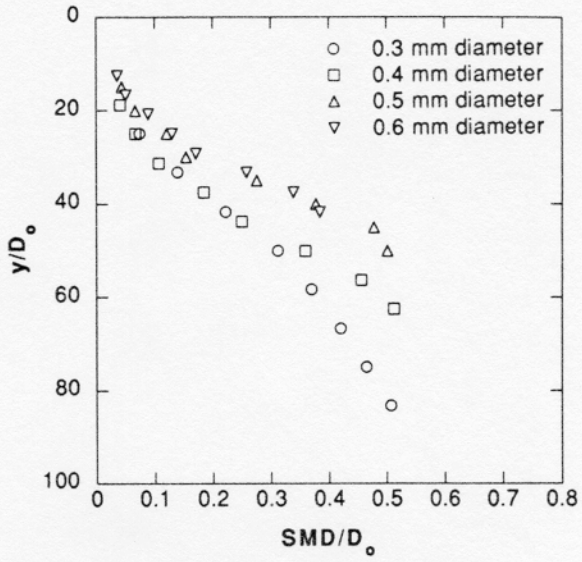

Fig. 11 SMD versus y for different orifice diameters under near identical relative velocities within 25 ± 1 m/s: x = 10 mm and Re_g = 70,000.

70,000, while the water flow rate is held constant at 2.10 ml/s through the 0.5-mm-diameter orifice and at x = 10 mm. At lower ALR, the stronger water momentum compared with the air momentum develops the jet to penetrate deeper into the air flow. Consequently, the spray SMD gradually decreases with decreasing ALR because of the enhanced atomization

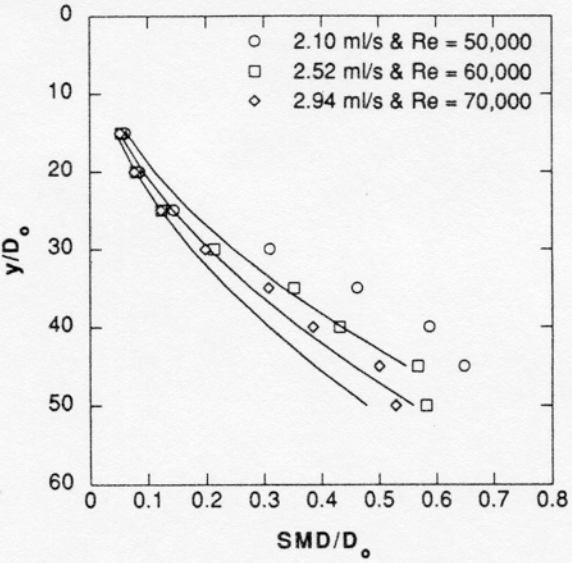

Fig. 12 SMD versus y for different Re_g under the same ALR of 25: x = 10 mm and D_o = 0.5 mm.

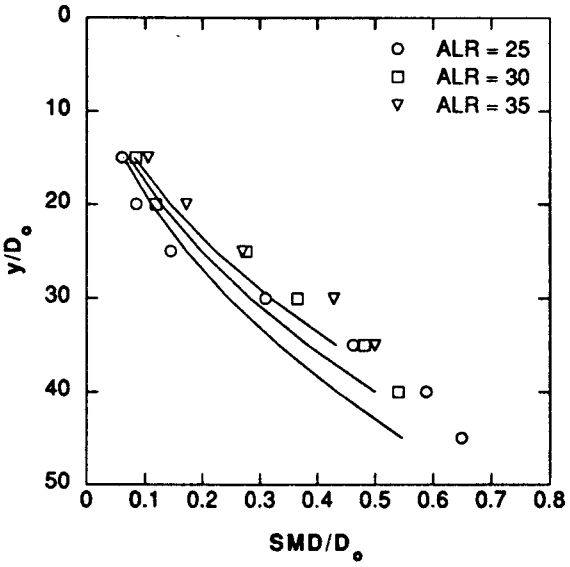

Fig. 13 SMD versus y for different ALRs ranging from 25 to 35: x = 10 mm, D_o = 0.5 mm, and $\dot{m}_f$ = 2.10 ml/s.

with the higher penetration. The effect of penetration, which decreases with increasing ALR and contributes to an increase in SMD, seems to override the adverse effect of the relative velocity, which increases with increasing ALR and reduces the SMD.

Effects of Measurement Location

Measurements at two different x locations, 10 and 20 mm downstream of the nozzle, were taken to inspect the spray SMD variation along the air-flow direction. A decrease in SMD along with the air flow is observed for the case of 1.58 ml/s of water flow rate through a 0.4-mm injector and Re_g = 70,000 (Fig. 14). Although not shown, cases with different orifices and at different injection rates show similar decreases in SMD along with the x coordinate. The air in a conventional air-blast atomizer is blown in parallel to the injected liquid, where the spray SMD gradually increases along the spray axis because of the enhanced coalescence of drops as their travel distance increases [22]. Preferential evaporation of smaller drops also contributes to an increasing SMD along the spray axis. However, the distinctively different drop paths in cross injection allow two-dimensional development of drop size distribution in both the x and y directions. Larger drops penetrate farther into the y direction as x increases and leave smaller drops downstream at the same y coordinate. This depletion of larger drops associated with the spray penetration as x increases attributes to the SMD decrease along the same y coordinate.

SUMMARY AND CONCLUSIONS

Drop size measurements using a laser diffraction technique have been reported for cross-injecting sprays with distilled water as an injected liquid. A comprehensive correlation

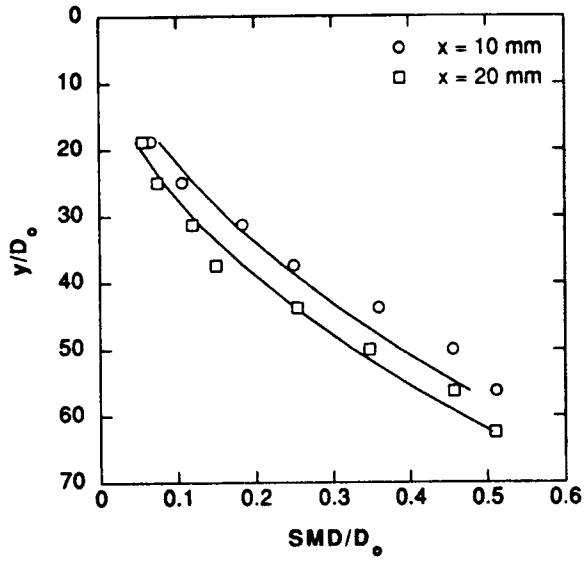

Fig. 14 SMD versus y measured at different x locations: D_o = 0.4 mm, $\dot{m}_f$ = 1.58 ml/s, and Re_g = 70,000.

of drop SMD is obtained from the experimental data in terms of the orifice diameter, gas Reynolds number, liquid Reynolds number, Weber number, and x and y positions. Several important discoveries have been made regarding the drop SMD characteristics. The SMD decreases as both gas and liquid Reynolds numbers increase. However, SMD gradually increases with increasing air-to-liquid (ALR) ratio. This is caused by the dominant role of the degree of spray penetration in determining the atomization characteristics of cross-injecting sprays. SMD increases with increasing Weber number and increasing penetration in the normal direction, y, but decreases along the axial direction, x.

APPENDIX: DIMENSIONAL ANALYSIS BASED ON BUCKINGHAM PI THEOREM

Sauter mean diameter (SMD) with respect to the orifice diameter is thought to be a function of the velocity, density, and viscosity of the air, the velocity, density, viscosity, and surface tension of the water, and position in the spray. This is shown by

$$\text{SMD} = f\left(D_o, V_g, \rho_g, \mu_g, V_f, \rho_f, \mu_f, \sigma, x, y\right) \tag{A1}$$

where the SMD is in μm, the orifice diameter D_o is in mm, the air velocity V_g is in m/s, the air density ρ_g is in kg/m^3, the air viscosity μ_g is in kg/m s, the water velocity V_f is in m/s, the water density ρ_f is in kg/m^3, the water viscosity μ_f is in kg/m s, the water surface tension σ is in N/m, and the x and y coordinates are in mm.

The Buckingham-PI theorem is used to nondimensionalize the function for SMD. Eight PI groups are obtained from the variables:

$$\pi_1 = \frac{\text{SMD}}{D_o} \qquad \pi_2 = \frac{x}{D_o} \qquad \pi_3 = \frac{y}{D_o} \qquad \pi_4 = \frac{\rho_g V_g D_o}{\mu_g}$$

$$\pi_5 = \frac{\rho_g V_g^2 D_o}{\sigma} \qquad \pi_6 = \frac{V_g}{V_f} \qquad \pi_7 = \frac{\rho_g}{\rho_f} \qquad \pi_8 = \frac{\rho_f V_f D_o}{\mu_f} \tag{A2}$$

By means of dimensional analysis, the following equation is derived:

$$\frac{\text{SMD}}{D_o} = A\left(\frac{\rho_g V_g D_o}{\mu_g}\right)^B \left(\frac{\rho_g V_g^2 D_o}{\sigma}\right)^C \left(\frac{V_g}{V_f}\right)^E \left(\frac{\rho_g}{\rho_f}\right)^F \left(\frac{x}{D_o}\right)^H \left(\frac{y}{D_o}\right)^I \left(\frac{\mu_g}{\mu_f}\right)^J \left(\frac{\rho_f V_f D_o}{\mu_f}\right)^K \tag{A3}$$

where A is a proportionality constant. In this investigation the velocities, densities, and viscosities are not examined directly, so the terms representing their ratios are eliminated. Note here that the elimination of these ratios limits the applicability of the present correlation to those fluids with viscosity values approximately the same as water.

For convenience, the term in the first parenthesis on the right-hand side of Eq. (A3) has been modified by replacing the length scale of D_o with D_H. The SMD-to-D_o ratio is expressed as a function of the air flow Reynolds number, the liquid flow Reynolds number, the Weber number, the x-to-D_o ratio, and the y-to-D_o ratio:

$$\frac{\text{SMD}}{D_o} = A\,\text{Re}_g^B\,\text{Re}_f^K\,\text{We}^C\left(\frac{x}{D_o}\right)^H\left(\frac{y}{D_o}\right)^I \tag{A4}$$

where A, B, K, C, H, and I are constants to be determined.

In order for Eq. (A4) to be solved by a least-squares method associated with experimental data, it must be linearized by applying the log function to both sides of the equation. The resulting equation takes the form

$$\log\left(\frac{\text{SMD}}{D_o}\right) = \log(A) + B\log\left(\text{Re}_g\right) + K\log\left(\text{Re}_f\right) + C\log(\text{We}) + H\log\left(\frac{x}{D_o}\right) + I\log\left(\frac{y}{D_o}\right) \tag{A5}$$

Because A is the same for all cases, $\log(A)$ is substituted by another constant called L. Equation (A5) now becomes

$$\log\left(\frac{\text{SMD}}{D_o}\right) = L + B\log\left(\text{Re}_g\right) + K\log\left(\text{Re}_f\right) + C\log(\text{We}) + H\log\left(\frac{x}{D_o}\right) + I\log\left(\frac{y}{D_o}\right) \tag{A6}$$

The equation is now linear with respect to the unknown constants L, B, K, C, H, and I. The linear least-squares statistical method is used to solve for the constants from all of the experimental data.

REFERENCES

1. R. D. Ingebo, and H. F. Foster, Drop-Size Distribution for Crosscurrent Breakup of Liquid Jets in Airstreams, National Advisory Committee for Aeronautics Rept., TN4087, 1957.
2. K. D. Kihm, D. P. Terracina, S. E. Payne, and J. A. Caton, Synchronized Drop Size Measurements for Coal-Water Slurry Sprays Generated from a High-Pressure Diesel Injection System, *J. Inst. Energy*, vol. 67, pp. 2–9, 1994.
3. M. Adelberg, Breakup Rate and Penetration of a Liquid Jet in a Gas Stream, *AIAA J.*, vol. 5, pp. 1408–1415, 1967.
4. N. A. Chigier, The Physics of Atomization, Interim Report, Department of Mechanical Engineering, Carnegie Mellon University, Pittsburgh, PA, 1991.
5. M. Adelberg, Mean Drop Size Resulting from the Injection of a Liquid Jet into a High Speed Gas Stream, *AIAA J.*, vol. 6, pp. 1143–1147, 1968.
6. J. F. Keffer and W. D. Baines, The Round Turbulent Jet in a Cross-Wind, *J. Fluid Mech.*, vol. 15, pp. 481–496, 1962.
7. Y. Kamotani and I. Greber, Experiments on a Turbulent Jet in a Cross Flow, *AIAA J.*, vol. 10, pp. 1425–1429, 1972.
8. Z. M. Moussa, J. W. Trischka, and S. Eskinazi, The Near Field in the Mixing of a Round Jet with a Cross-Stream, *J. Fluid Mech.*, vol. 80, pp. 49–80, 1977.
9. J. E. Broadwell and R. E. Breidenthal, Structure and Mixing of a Transverse Jet in Incompressible Flow, *J. Fluid Mech.*, vol. 148, pp. 405–412, 1984.
10. J. Andreopoulos, On the Structure of Jets in a Cross Flow, *J. Fluid Mech.*, vol. 157, pp. 163–197, 1985.
11. S. D. Heister, T. T. Nguyen, and A. R. Karagozian, Modeling of Liquid Jets Injected Transversely into a Supersonic Cross Flow, *AIAA J.*, vol. 27, pp. 1727–1732, 1988.
12. D. J. Needham, N. Riley, and J. H. B. Smith, A Jet in Cross Flow, *J. Fluid Mech.*, vol. 188, pp. 159–184, 1988.
13. D. J. Needham, N. Riley, C. C. Lytton, and J. H. B. Smith, A Jet in Cross Flow. Part 2, *J. Fluid Mech.*, vol. 211, pp. 515–528, 1990.
14. A. Askari, S. J. Bullman, M. Fairweather, and F. Swaffield, The Concentration Field of a Turbulent Jet in a Cross-Wind, *Combustion Sci. Technol.*, vol. 73, pp. 463–478, 1990.
15. H. S. Li and A. R. Karagozian, Breakup of a Liquid Jet in Supersonic Cross Flow, AIAA Paper 91-0689, 1991.
16. T. J. Benson and S. W. Kim, Calculation of a Circular Jet in Cross Flow with a Multiple-Time-Scale Model, *Int. J. Heat Mass Transfer*, vol. 35, no. 10, pp. 2357–2365, 1992.
17. F. J. Higuera and M. Martinez, An Incompressible Jet in a Weak Cross Flow, *J. Fluid Mech.*, vol. 249, pp. 73–95, 1993.
18. A. H. Lefebvre, *Atomization of Sprays*, Hemisphere, New York, NY, 1989.
19. L. G. Dodge, Southwest Research Institute, San Antonio, TX, personal communication, 1990.
20. S. J. Kline, The Purposes of Uncertainty Analysis, *J. Fluids Eng.*, vol. 107, pp. 153–160, 1985.
21. G.M. Lyn, *Drop-Size Distribution for Crosscurrent Breakup of a Liquid Jet in a Convective Airstream*, M.S. thesis, Texas A&M University, College Station, TX, 1994.
22. K. D. Kihm and N. Chigier, Effect of Shock Waves on Liquid Atomization of a Two-Dimensional Airblast Atomizer, *Atomization and Sprays*, vol. 1, no.1, pp. 113–136, 1991.